

Low Weber number jet collision regimes in microgravity

Francesc Suñol and Ricard González-Cinca

*Department of Physics, Universitat Politècnica de Catalunya - BarcelonaTech,
c/ E. Terradas 5, 08860 Castelldefels, Barcelona, Spain*

(Dated: November 3, 2017)

The outcome of the collision between two liquid jets depends on the liquid properties, jet velocity and impact angle. So far studies on liquid jet impingement have been carried out in normal gravity conditions. In microgravity, jets are not accelerated and can show a different behavior than on ground. We perform an experimental analysis of the injection of liquid jets in microgravity, focusing in the jet impingement at different velocities and impact angles at low Weber number. Several regimes are obtained, some of which are not observable on ground. Other regimes take place at different parameters ranges than in normal gravity. A map of the observed regimes is proposed in terms of the Weber number and the impact angle.

PACS numbers: 47.55.df, 47.15.Uv, 47.55.N-

INTRODUCTION

The collision between two liquid jets can result in merging, bouncing, or dispersion in form of droplets [1–3]. The outcome of the collision can be controlled by changing two parameters, namely the flow rate and the impact angle of the colliding jets. Hence, the impinging jets configuration with changeable orientation becomes a simple and flexible method to enhance mixing. This configuration can be found in a variety of applications such as propellant injection in rocket engines, agrochemical coating, ink-jet printing, as well as in several pharmaceutical processes.

Most studies on liquid jets have focused on the description of the jet breakup mechanisms and the resulting droplet characteristics. The pioneering work of Lord Rayleigh on the linear stability analysis around the cylindrical base state was followed by numerous works considering non-linear effects that can become dominant in the breakup process. Very complete reviews of the underlying physics behind the jet breakup mechanisms can be found in Lin [4] and Eggers and Villermaux [5]. Three modes of liquid behaviour with their associated breakup mechanisms can take place in the laminar regime in normal gravity conditions: periodic dripping, chaotic dripping and jetting. Many attempts to model the breakup of liquid filaments or the transition between different regimes have been carried out [6–14]. Gravity force is neglected in most models, even though gravity can affect the jet breakup in cases like low surface tension fluids. Different modes of liquid jetting have been found in experiments in microgravity conditions [15, 16]. Umemura and Wakashima [17] and Tsukiji et al. [18] studied the atomization regimes of a liquid jet in weightlessness, as well as the effects of pressure and temperature. Suñol and González-Cinca [19, 20] reported a quantitative analysis of the breakup length, droplet size and jet structure in the breakup of a liquid jet in microgravity.

When two liquid jets collide, they can coalesce forming

a new jet, a liquid chain or a sheet; bounce off each other; or disintegrate in the form of small droplets. The critical element determining merging versus bouncing is the dynamics of the air film that separates the colliding interfaces. Jets can attract and coalesce when the thickness of the film is reduced to the range of the intermolecular van der Waals forces (of the order of 100 nm). Li et al. [21] identified soft and hard merging mechanisms of colliding jets. In addition, they demonstrated that bouncing is confined to regimes of low Stokes number and high ratio between jet and capillary waves velocity. These regimes represent weak impact inertia and weak capillary effects, respectively. Given the dependence of these effects on liquid properties, bouncing in water was predicted to be non observable at atmospheric conditions. Wadha et al. [22] captured qualitatively the transition of colliding jets from bouncing to coalescence by means of a parameter determined by the Weber and Reynolds numbers as well as the angle of collision. All the studies carried out until now belong to the inertia-dominated regime achieved under normal gravity conditions. The collision between liquid jets in microgravity conditions has not been addressed yet, even though the non-accelerated jets could give rise to new phenomenologies of potential interest for the design of space systems such as low-thrust satellite positioners and the operation of bipropellant rocket engines.

At high Weber number, the effects of gravity force on the collision between jets can be neglected since the acceleration generated to the jets is very low compared to the change in velocity caused by the collision. Thus, experiments in a microgravity environment are not expected to provide any new understanding on the characteristics of liquid jet collisions at high Weber number. However, at low Weber number, microgravity conditions are necessary to maintain the symmetry of the collision configuration.

In the present study, we analyze the injection of liquid jets in microgravity conditions, with a particular empha-

92 sis in the impingement of jets at different velocities and
 93 collision angles. Our aim is to determine the regimes that
 94 take place at low Weber number $We = \rho d_n v^2 / \sigma$, where
 95 ρ is the liquid density, d_n is the nozzle diameter, v is the
 96 velocity, and σ is the surface tension, and to compare
 97 them with results in normal gravity conditions.

98 EXPERIMENTAL SETUP

99 In order to carry out experiments in microgravity con-
 100 ditions, an experimental setup was designed to be used
 101 at the ZARM drop tower. In this platform, setups are
 102 placed inside an airtight capsule (1.5 m long and 80
 103 cmwide) that is pulled up to a height of 120 meters at
 104 the top of the drop tube and released. After 4.74 s,
 105 the experiment lands in the deceleration unit filled with
 106 polystyrene pellets. During the free fall, the pressure
 107 inside the drop tube is 10^{-5} atm. The low air resis-
 108 tance allows the ZARM drop tower to provide a very
 109 good quality of microgravity of approximately $10^{-6} g_0$,
 110 where $g_0 = 9.81$ m/s² is the gravity acceleration at sea
 111 level.

112 Distilled water ($\rho = 998$ kg/m³, $\sigma = 7.28 \cdot 10^{-2}$ N/m²)
 113 was injected from two nozzles ($d_n = 1$ mm) at variable
 114 orientation and flow rate. The impact angle 2α of the jets
 115 was changed from 6° (quasi-parallel jets) to 180° (frontal
 116 collision). The flow rate at each nozzle Q varied from 5
 117 to 100 ml/min, which corresponds to $0.5 \leq We \leq 62$.

118 The flow rate was controlled and maintained by a high-
 119 accuracy liquid pump (Ismatec MCP-Z Standard), which
 120 assured a constant flow at each nozzle in microgravity
 121 conditions. A T-junction bifurcated the flow into two
 122 sub-lines, each of them connected to a manual valve that
 123 compensated any irregularities in the flow split at the
 124 T-junction. Images were recorded by means of a high-
 125 speed camera (Photron FastCam MC2) at 1000 fps with
 126 a resolution of 512x512 pixels each frame. Both the flow
 127 rate and the high-speed camera were controlled remotely
 128 using LabView software.

129 RESULTS AND DISCUSSION

130 The breakup length L_b of a single jet was obtained
 131 over $N = 500$ frames for every Q , and the average value
 132 $\langle L_b \rangle = \frac{1}{N} \sum_{i=1}^N L_{bi}$ was calculated. The breakup length
 133 shows a linear behaviour with the jet velocity (hence with
 134 \sqrt{We}) at a wide range of flow rates [4].

135 Figure 1 shows the normalized average breakup length
 136 as a function of \sqrt{We} . Labels “a” and “b” correspond
 137 to the dripping regime, in which the injected droplet re-
 138 mains attached to the nozzle. In “a”, inertia is negligible
 139 and the droplet shape remains approximately spherical.
 140 As the flow rate increases, inertia forces slightly prevail
 141 over surface tension, which makes the droplet to adopt

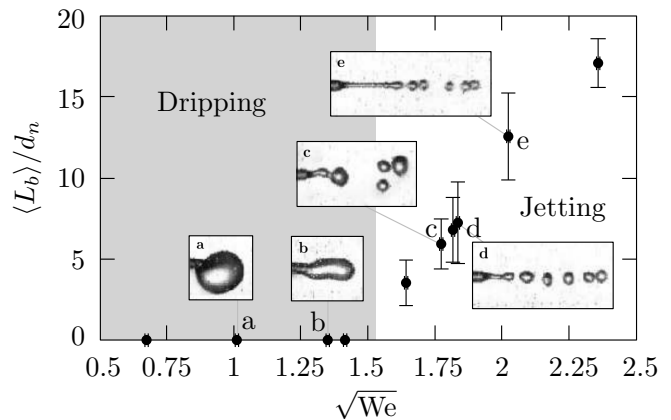


FIG. 1. Normalized average breakup length as a function of \sqrt{We} . “a” and “b” correspond to the dripping regime (liquid mass attached to the nozzle), while “c”, “d” and “e” correspond to the jetting regime.

142 an irregular elongated shape (“b”). When inertia over-
 143 comes surface tension, a liquid jet is formed (“c”, “d”
 144 and “e” in Fig. 1). The transition from dripping to jet-
 145 ting occurs at a critical Weber ($We_{cr} \approx 2.3$). At low
 146 flow rates in the jetting regime ($We \gtrsim We_{cr}$), the droplet
 147 size and generation frequency are highly unpredictable
 148 (“c”). As the flow rate increases, the droplets generated
 149 from the jet breakup become smaller and with a lower
 150 size dispersion (“d” and “e”). In this case, the average
 151 jet breakup length increases linearly with the square root
 152 of the Weber number [20].

153 A wide range of regimes emerge as a result of the
 154 oblique and frontal jet interactions (see in Table I all
 155 the cases studied, where v is the liquid injection veloc-
 156 ity). Figure 2 shows the regimes obtained in the oblique
 157 jet interaction. In Figs. 2a and 2d, a nonuniform spatial
 158 distribution of noncoalescing droplets is generated. Figs.
 159 2b and 2e show droplets from different jets coalescing
 160 with each other. Soft merging between low velocity jets
 161 with a sudden bend of the jets very close to the merging
 162 point can be observed in Figs. 2c and 2f. Hard merging
 163 takes place at high impact inertia, giving rise to a liquid
 164 chain (Fig. 2g) or a sheet (Fig. 2h and 2i). At low values
 165 of 2α used ($6^\circ \leq 2\alpha \leq 22^\circ$), jets bounced off each other
 166 with an outgoing angle 2ϕ smaller than the impact angle
 167 (Figure 2j). The non coalescence between jets can be re-
 168 lated to the behaviour of the film of air separating both
 169 interfaces as they come close to each other, as found in
 170 [22]. Jets drag along air into the collision region, where
 171 it is squeezed in a thin film. Since the thickness of the
 172 air film is much smaller than the other dimensions, lubri-
 173 cation approximation is applicable, which results in high
 174 magnitude forces keeping the jets apart. As soon as the
 175 air between jets is drained out, coalescence could take
 176 place.

177 The transition from jet bouncing to coalescence is il-

Fig#	2α (degrees)	v (m/s)	Regime
2a	82	0.49	Droplet bouncing
2b	82	0.55	Droplet coalescence
2c	82	0.74	Jet coalescence
2d	14	0.49	Droplet bouncing
2e	14	0.53	Droplet coalescence
2f	14	0.59	Jet coalescence
2g	30	2.12	Liquid chain
2h	90	1.34	Liquid chain/sheet
2i	90	2.12	Liquid sheet
2j	10	0.68	Jet bouncing
3	22	0.68	Jet coalescence/bouncing
6a	180	0.38	Dripping
6b	180	0.45	Droplet bouncing
6c	180	0.47	Droplet bouncing
6d	180	0.64	Jet coalescence
6	6	0.62	Jet coalescence
6	6	0.85	Jet coalescence/bouncing
53	6	0.70	Jet coalescence
180	180	0.49	Droplet coalescence
180	180	0.53	Droplet coalescence
180	180	0.91	Jet coalescence
180	180	2.12	Liquid sheet

TABLE I. List of analyzed cases.

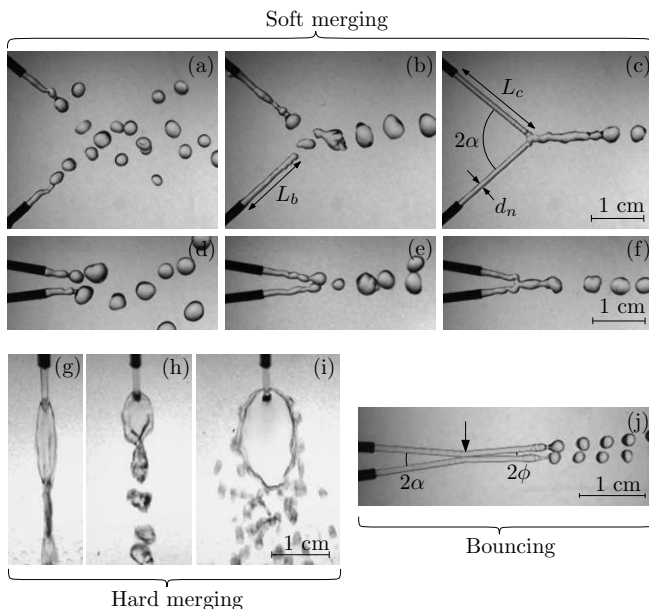


FIG. 2. Snapshots of different regimes when oblique jets are injected. (a) and (d) droplet bouncing; (b) and (e) droplet coalescence; (c) and (f) jet coalescence; (g) liquid chain; (h) and (i) liquid sheet; (j) jet bouncing. (a)-(f) soft merging; (g)-(i) hard merging.

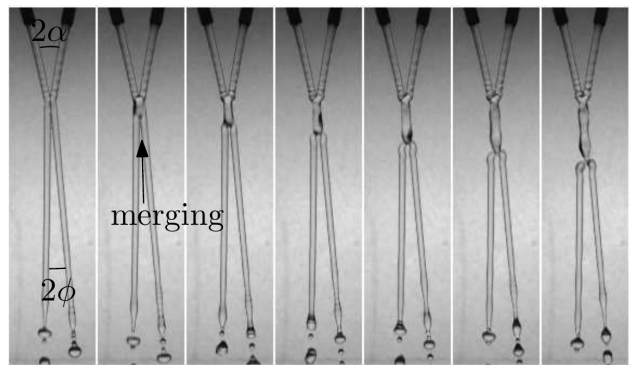


FIG. 3. Series of snapshots showing the transition from bouncing to coalescing jets. Time interval between consecutive frames is 1 ms.

184 (which can be due to nozzle vibrations, pump anomalous
185 operation, or the presence of a colloid in the liquid) can
186 force the air to quickly drain out giving rise to coales-
187 cence.

188 Due to the symmetry of the problem, the dynamics
189 of the air layer between colliding jets is analogous to
190 that of the droplet impact on solid surfaces [21]. The
191 width of the air layer H_d scales with the dimensionless
192 impact velocity as $H_d/R = A_I St^{-2/3}$, where $R = d_n/2$,
193 A_I is a prefactor, and St is the Stokes number, defined
194 as $St = \rho R v / \eta_g$, where $\eta_g = 1.983 \cdot 10^{-5}$ Pa s is the
195 air viscosity. When oblique collisions are considered, the
196 impact velocity is modified by a $\sin \alpha$ factor. Thus, the
197 Stokes number becomes $St = \rho d_n v \sin \alpha / (2\eta_g)$. Accord-
198 ing to Li *et al.* [21], there is a critical value of the Stokes
199 number that determines the transition from bouncing to
200 merging. At low jet velocities, the shape of the jet is
201 not cylindrical due to the reflected waves to the nozzle.
202 The velocity of the capillary waves is estimated as
203 $v_c \approx (\sigma k / \rho)^{1/2}$, where k is the wavenumber and is of the
204 order of $1/R$. The ratio between the jet velocity and the
205 capillary waves velocity leads to a second dimensionless
206 number Γ , defined as $\Gamma = v / v_c = v(\rho R / \sigma)^{1/2}$, which
207 controls the bouncing/merging transition at low jet ve-
208 locities [21]. Therefore, the jet bouncing and coalescence
209 regimes can be analyzed by means of the Stokes number
210 St and the ratio between jet and capillary waves velocity
211 Γ . Fig. 4 shows St as a function of Γ . Crosses correspond
212 to coalescence, circles to bouncing, and crosses inside circles
213 to a metastable bouncing state like the one shown in
214 Fig. 3. Jet bouncing was found only at $\Gamma > 0.2$ in [21].
215 However, two of the observed bouncing regimes in our ex-
216 periments took place at $\Gamma < 0.2$. Therefore, microgravity
217 conditions seem to favour bouncing against coalescence.
218 Bouncing is enhanced in microgravity since jets are not
219 accelerated and hence the removal of air between them
220 becomes more difficult.

178 lustrated in Fig. 3. The bouncing regime corresponds
179 to a metastable state, and coalescence is triggered by an
180 instability in the interface of the colliding jets. A film
181 of air is entrained by the liquid flow and is continuously
182 replenished, resulting in a self-sustained noncoalescence.
183 However, a sufficiently large perturbation in the jet flow

221 The transition from bouncing to coalescence can be
222 analyzed in terms of the parameter K , defined as

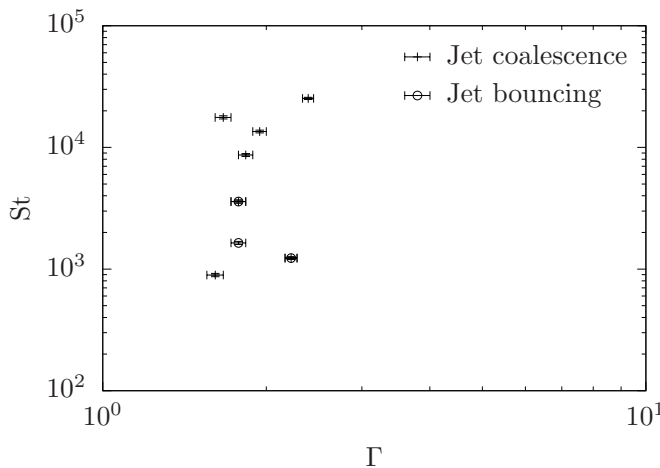


FIG. 4. Stokes number as a function of the ratio between jet and capillary waves velocity.

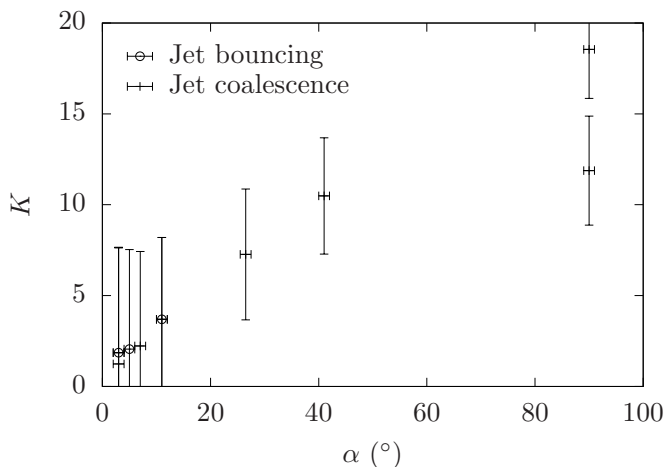


FIG. 5. $K = (We_\alpha \sqrt{Re_\alpha} / \sin \alpha)^{1/2}$ as a function of the impact angle.

223 $K = (We_\alpha \sqrt{Re_\alpha} / \sin \alpha)^{1/2}$, where $We_\alpha = We \sin^2 \alpha$ and
 224 $Re_\alpha = v d_n \sin \alpha / \nu$, ν being the kinematic viscosity. The
 225 introduction of the dimensionless numbers We_α and Re_α
 226 comes when considering oblique collisions, since the im-
 227 pact velocity becomes $v \sin \alpha$. Wadhwa et al. observed
 228 coalescence at $K > K_{cr}$ and bouncing at $K < K_{cr}$, with
 229 $K_{cr} = 6.1$ [22]. Fig. 5 shows the behaviour of K as a
 230 function of α for the cases of jet bouncing and coalescence
 231 observed here, where a cross inside a circle corresponds
 232 to a metastable bouncing state. Our results show several
 233 cases of jet coalescence at $K < 6.1$ at $\alpha < 10^\circ$, which
 234 is a region not explored in [22]. In this region jets are
 235 quasi-parallel and small interfacial instabilities can gen-
 236 erate coalescence more easily than at large values of α .
 237 In fact, one would expect that in normal gravity condi-
 238 tions this effect is enhanced and that K_{cr} substantially
 239 decreases as $\alpha = 0^\circ$ is approached.

240 The frontal collision between two jets provides partic-

241 ular features since the system is axisymmetric and the
 242 outcome of the collision is located in the injection axis.
 243 As a consequence, the resulting fluid body interacts with
 244 the incoming liquid streams, as opposed to the oblique
 245 jets case, in which the result of the collision moves away
 246 from the collision point. Fig. 6 shows the regimes ob-
 247 served in the opposed-jets configuration, with a separa-
 248 tion between nozzle tips of 6 cm. Fig. 6a shows the
 249 dripping regime that takes place at low We , in which
 250 surface tension dominates over fluid inertia and droplets
 251 grow remaining attached to the nozzles. In Figs. 6b to
 252 6d, $We > We_{cr}$ and the jetting mode is attained. Fig.
 253 6b shows the dispersion of droplets generated from jet
 254 atomization occurring close to the nozzle. Droplets ap-
 255 proach each other at a relative velocity around 10 cm/s
 256 and bounce off since the time scale of draining the air
 257 film between the two interfaces is higher than the con-
 258 tact time between droplets. At higher jet velocities, the
 259 inertia of the colliding droplets generates strong pertur-
 260 bations of the air gap between liquid interfaces, forcing
 261 them to coalesce. In this case, a central droplet is formed
 262 and grows from coalescence with incoming droplets (Fig.
 263 6c). The jet breakup length increases with increasing
 264 flow rate. When L_b is larger than the distance from the
 265 nozzle tip to the collision point, jets coalesce before at-
 266 omization can take place, and a liquid bridge is formed
 267 (Fig. 6d). The interaction between jets creates a central
 268 liquid body that connects the two nozzles permanently.
 269 The shape of the liquid bridge highly depends on the flow
 270 rate. At low flow rates, the bridge shape oscillates be-
 271 tween oblate and prolate spheroids. At large flow rates,
 272 the central body becomes a steady liquid sheet.

273 To characterize the conditions under which the ob-
 274 served regimes take place, a map in terms of the Weber
 275 number and the impact angle is proposed (Fig. 7). The
 276 regimes represented, ordered by increasing flow rate, are:
 277 dripping, droplet bouncing, droplet coalescence, jet co-
 278 alence, jet bouncing, liquid chain, and liquid sheet.

279 Some of the regimes, such as jet bouncing or liquid
 280 chains, occur only in configurations with $2\alpha \neq 0, \pi$ rad.
 281 Jet coalescence is observed at $\alpha = 0$ rad as a result of
 282 the soft merging mechanism.

CONCLUSIONS

284 In conclusion, our results significantly extend the un-
 285 derstanding of the behavior of liquid jets at low Weber
 286 numbers. We have analyzed the impingement of jets in
 287 microgravity conditions in a large range of impact angle
 288 including frontal collision, and observed several regimes.
 289 Some of the regimes take place at different parameters
 290 ranges that in normal gravity conditions, while others oc-
 291 cur only in microgravity. A map of the identified regimes
 292 have been proposed in terms of the Weber number and
 293 the impact angle.

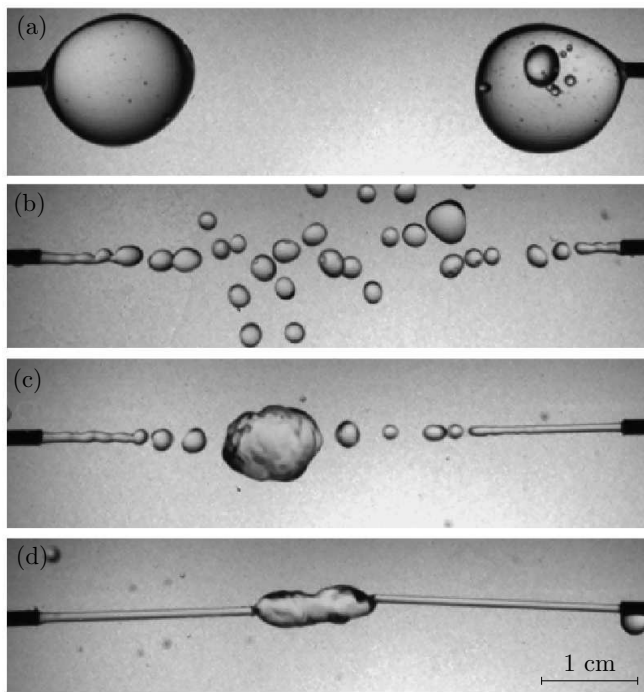


FIG. 6. Regimes observed in the opposed-jets configuration: (a) dripping; (b) droplet bouncing; (c) droplet coalescence; (d) jet coalescence.

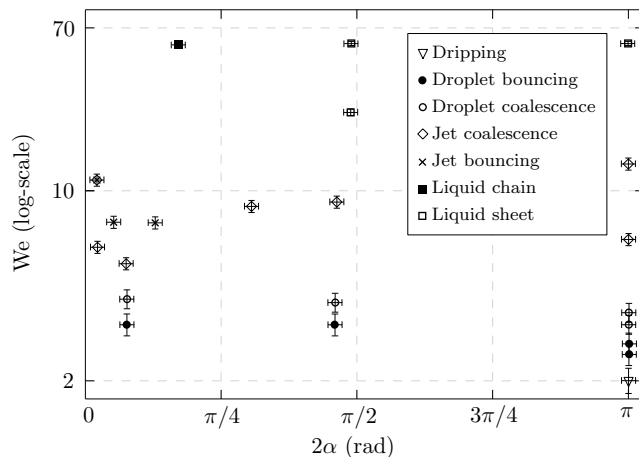


FIG. 7. Jet collision regimes in terms of We and the impact angle.

294

ACKNOWLEDGEMENTS

295 This research was supported by the Spanish *Ministe-*
 296 *rio de Economía y Competitividad, Secretaría de Estado*
 297 *de Investigación, Desarrollo e Innovación* (project num-
 298 ber AYA2012-34131), and by the *Agencia Estatal de In-*
 299 *vestigación* and EU FEDER (project number ESP2016-
 300 79196-P). We acknowledge ESA for providing access to
 301 the ZARM drop tower, and ZARM engineers for their
 302 technical assistance.

- 303 [1] Y.J. Choo and B.S. Kang, “A study on the velocity char-
 304 acteristics of the liquid elements produced by two imping-
 305 ing jets,” *Experiments in Fluids* **34**, 655–661 (2003).
 306 [2] Sungjune Jung, Stephen D. Hoath, Graham D. Martin,
 307 and Ian M. Hutchings, “Atomization patterns produced
 308 by the oblique collision of two newtonian liquid jets,”
 309 *Physics of Fluids* **22**, 042101 (2010).
 310 [3] Navish Wadhwa and Sunghwan Jung, “Non-coalescence
 311 of jets,” *Physics of Fluids* **23**, 091105 (2011).
 312 [4] S. P. Lin, *Breakup of liquid sheets and jets* (Cambridge
 313 University Press, 2003).
 314 [5] Jens Eggers and Emmanuel Villermaux, “Physics of liq-
 315 uid jets,” *Reports on Progress in Physics* **71**, 036601
 316 (2008).
 317 [6] R. D. Reitz and F. V. Bracco, “Mechanism of atomization
 318 of a liquid jet,” *Physics of Fluids* **25**, 1730–1742 (1982).
 319 [7] S. J. Leib and M. E. Goldstein, “Convective and absolute
 320 instability of a viscous liquid jet,” *Physics of Fluids* **29**,
 321 952–954 (1986).
 322 [8] S. P. Lin and Z. W. Lian, “Absolute instability of a liquid
 323 jet in a gas,” *Physics of Fluids* **1**, 490–493 (1989).
 324 [9] S. P. Lin and R. D. Reitz, “Drop and spray formation
 325 from a liquid jet,” *Annual Review of Fluid Mechanics*
 326 **30**, 85–105 (1989).
 327 [10] Bala Ambravaneswaran, Hariprasad J. Subramani,
 328 Scott D. Phillips, and Osman A. Basaran, “Dripping-
 329 jetting transitions in a dripping faucet,” *Phys. Rev. Lett.*
 330 **93**, 034501 (2004).
 331 [11] Wim van Hoeve, Stephan Gekle, Jacco H. Snoeijer,
 332 Michel Versluis, Michael P. Brenner, and Detlef Lohse,
 333 “Breakup of diminutive rayleigh jets,” *Physics of Fluids*
 334 **22**, 122003 (2010).
 335 [12] J. M. Montanero, M. A. Herrada, C. Ferrera, E. J. Vega,
 336 and A. M. Gañán Calvo, “On the validity of a universal
 337 solution for viscous capillary jets,” *Physics of Fluids* **23**,
 338 122103 (2011), <http://dx.doi.org/10.1063/1.3670007>.
 339 [13] A. M. Gañán Calvo, C. Ferrera, and J. M. Montanero,
 340 “Universal size and shape of viscous capillary jets: ap-
 341 plication to gas-focused microjets,” *Journal of Fluid Me-*
 342 *chanics* **670**, 427–438 (2011).
 343 [14] Alfonso A. Castrejón-Pita, J. R. Castrejón-Pita, and
 344 I. M. Hutchings, “Breakup of liquid filaments,” *Phys.*
 345 *Rev. Lett.* **108**, 074506 (2012).
 346 [15] A. P. R. Edwards, B. P. Osborne, J. M. Stoltzfus,
 347 T. Howes, and T. A. Steinberg, “Instabilities and drop
 348 formation in cylindrical liquid jets in reduced gravity,”
 349 *Physics of Fluids* **14**, 3432–3438 (2002).
 350 [16] Barnaby Osborne and Theodore Steinberg, “An experi-
 351 mental investigation into liquid jetting modes and break-
 352 up mechanisms conducted in a new reduced gravity fac-
 353 ility,” *Microgravity Science and Technology* **18**, 57–61
 354 (2006).
 355 [17] Akira Umemura and Yuichiro Wakashima, “Atomization
 356 regimes of a round liquid jet with near-critical mixing
 357 surface at high pressure,” *Proceedings of the Combustion*
 358 *Institute* **29**, 633 – 640 (2002).
 359 [18] H. Tsukiji, A. Umemura, and M. Hisida, “Micro-gravity
 360 research on the atomization mechanism of near-critical
 361 mixing surface jet,” *Proceedings of the Conference on*
 362 *Aerospace Propulsion* **44**, 97–101 (2004).

- 363 [19] Francesc Suñol and Ricard González-Cinca, “Droplet col- 370
364 lisions after liquid jet breakup in microgravity condi- 371
365 tions,” *Journal of Physics: Conference Series* **327**, 012026 372
366 (2011). 373
- 367 [20] Francesc Suñol and Ricard González-Cinca, “Liquid jet 374
368 breakup and subsequent droplet dynamics under normal 375
369 gravity and in microgravity conditions,” *Physics of Fluids* **27**, 077102 (2015).
- [21] Minglei Li, Abhishek Saha, D. L. Zhu, Chao Sun, and Chung K. Law, “Dynamics of bouncing-versus-merging response in jet collision,” *Phys. Rev. E* **92**, 023024 (2015).
- [22] Navish Wadhwa, Pavlos Vlachos, and Sunghwan Jung, “Noncoalescence in the oblique collision of fluid jets,” *Phys. Rev. Lett.* **110**, 124502 (2013).